

# Effects of Support Structure and Composition on the Activity of Cu–Ni Catalysts for Methanol Steam Reforming

A. A. Lytkina<sup>a, \*</sup>, N. A. Bakuleva<sup>a</sup>, N. V. Orekhova<sup>a</sup>, M. M. Ermilova<sup>a</sup>, and A. B. Yaroslavtsev<sup>a, b, c</sup>

<sup>a</sup>Topchiev Institute of Petrochemical Synthesis, Russian Academy of Sciences, Leninskii pr. 29, Moscow, 119991 Russia

<sup>b</sup>Kurnakov Institute of General and Inorganic Chemistry, Russian Academy of Sciences, Leninskii pr. 31, Moscow, 119071 Russia

<sup>c</sup>Higher School of Economics (National Research University), Myasnitskaya ul. 20, Moscow, 101000 Russia

\*e-mail: lytkina@ips.ac.ru

Received May 10, 2019; revised June 6, 2019; accepted June 21, 2019

**Abstract**—We have studied the catalytic activity of Cu–Ni bimetallic catalysts on yttrium-, tin-, zinc-, and niobium-doped zirconia and ceria supports for methanol steam reforming (MSR), a process for hydrogen production, and examined the effect of the nature of the dopants and annealing temperature on the structure and particle size of the oxide supports and the catalytic activity of the metal oxide composites. In all cases, the addition of heterovalent ions improved the catalytic activity of the materials for the MSR process in comparison with undoped zirconia. The highest hydrogen yield was reached in the case of catalysts doped with niobium and yttrium oxides.

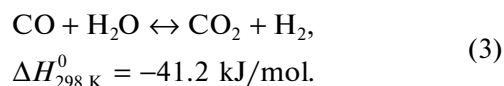
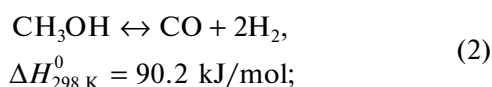
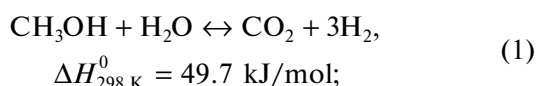
**Keywords:** methanol steam reforming, hydrogen production, bimetallic catalysts, oxide supports, support effect

**DOI:** 10.1134/S0020168519120100

## INTRODUCTION

Because of the environmental pollution with fuel combustion products, a search for new, environmentally friendly energy sources is becoming a more and more critical issue with every passing year. One promising approach is to produce electrical energy with the use of fuel cells. In connection with this, hydrogen is becoming one of the most highly demanded products for alternative power generation technologies [1–6]. However, it is rather difficult to transport and store. One solution to these problems is hydrogen production from liquid raw materials, such as lower alcohols [7–11].

Methanol steam reforming (MSR) takes place at relatively low temperatures (200–350°C) and has high hydrogen selectivity. The MSR process involves, in addition to the intended reaction (1), methanol decomposition reaction (2) and the reaction of the forming CO with water (3), resulting in the formation of a mixture of hydrogen, carbon dioxides, and a small amount of carbon monoxide:



The most frequently used catalysts are copper and Group VIII B metals, which offer high catalytic activity and hydrogen selectivity. One way of improving the stability of such catalysts and reducing their cost is by adding a second metal [12–16]. Catalytic systems in current use typically have the form of metal nanoparticles on a support, which often consists of oxides [17–22]. In such a case, according to a bifunctional mechanism, alcohol conversion steps occur on metal atoms, and the support provides centers for activation of the water, which emphasizes the importance of adequately choosing the support. The structure and chemical composition of a support make it possible to influence the activity and selectivity of the catalytic composite as a whole.

Zirconia is of considerable interest as a support of metallic catalysts for the MSR process [23–26]. In a number of studies, it was shown to act as a promoter for copper-containing catalysts [27]. Zirconia can exist in several crystalline polymorphs. A particular structure can be obtained by adjusting the heat treatment temperature and the nature and concentration of dopants [28]. Besides, the use of dopants leads to a higher disorder and mobility of the oxygen sublattice of zirconia and an increase in the number of active centers, presumably due to structural defects, on the

catalyst surface [29, 30]. Potentially attractive dopants include heterovalent ions ( $Y^{3+}$ ,  $Sc^{3+}$ ,  $Ca^{2+}$ , and  $Mg^{2+}$ ), whose presence leads to the formation of vacancies in a sublattice, which ensure high oxygen mobility, and elements capable of redox transformations, such as cerium and tin [31, 32]. Interest in  $SnO_2$  in heterogeneous catalysis is aroused primarily by its ability to act as an efficient catalyst for oxidation, especially in reactions involving CO [33], which we believe could improve the selectivity of catalysts for MSR. Niobium oxide serves a dual function: it increases the density of lattice defects and, despite its low redox activity, is capable of ensuring an increase in the activity of catalysts for oxidation and dehydrogenation reactions [34–37].

Previously, we studied Ni–Cu catalysts supported on zirconia with a tetragonal and a monoclinic structure [24]. The objectives of this work were to produce Ni–Cu bimetallic catalysts supported on zirconia and ceria doped with yttrium, tin, zinc, and niobium and test the resultant catalysts in methanol steam conversion in the temperature range 200–350°C.

## EXPERIMENTAL

**Synthesis of catalysts, physicochemical characterization, and catalytic experiments.** Undoped zirconia was prepared via precipitation with a concentrated ammonium hydroxide solution from zirconyl nitrate,  $ZrO(NO_3)_2$  (99%, Aldrich), at pH 9 as described in detail previously [38].  $ZrO_2-0.1Y_2O_3$ ,  $ZrO_2-0.1SnO_2$ ,  $ZrO_2-0.1ZnO$ ,  $ZrO_2-0.1Nb_2O_5$ , and  $CeO_2-0.1SnO_2$  samples were prepared by a similar procedure, via precipitation from zirconyl nitrate,  $ZrO(NO_3)_2$  (99%, Aldrich); cerium nitrate,  $Ce(NO_3)_3 \cdot 6H_2O$  (99.995%); yttrium nitrate,  $Y(NO_3)_3 \cdot 6H_2O$  (reagent grade); tin(IV) chloride,  $SnCl_4 \cdot 5H_2O$  (98%, Aldrich), niobium chloride,  $NbCl_5$  (99.8%, Acros); and zinc acetate,  $Zn(CH_3COO)_2 \cdot 2H_2O$  (analytical grade, Aldrich). The hydrous oxides obtained in the first step were annealed in air for 5 h at a temperature of 400°C in a muffle furnace to ensure crystal structure formation. To assess the effect of annealing temperature on the physicochemical characteristics of the materials, some of them were further annealed at 800°C.

The resultant samples were sequentially impregnated with aqueous solutions of  $Cu(NO_3)_2 \cdot 3H_2O$  (>98%) and  $Ni(NO_3)_2 \cdot 6H_2O$  ( $\geq 98.5\%$ , Aldrich). The amounts of the solutions were adjusted so that the total metal content was 20% of the weight of the support. The nickel : copper ratio in the samples was 1 : 4, which was optimal for the Cu–Ni system according to previously reported data [24]. The suspension thus prepared was dispersed by ultrasonication for 1 h. Next, the excess water was evaporated at 100°C in a drying oven. The resultant catalysts were annealed in air at 400°C for 3 h and in a flow of 5%  $H_2/Ar$

(20 mL/min) for 3 h at 350°C in order to reduce the metals. According to electron probe microanalysis data, the nickel : copper ratio in all of the samples was near the intended value.

The specific surface area and pore size of the supports and catalysts were determined by BET measurements with an ASAP-2020N porosimeter (Micromeritics, the United States). The phase composition of the samples was determined by X-ray diffraction on a Rigaku D/MAX 2200 diffractometer ( $CuK_{\alpha_1}$  radiation). For data processing and qualitative analysis, we used Rigaku Application Data Processing software. The crystallite (coherent scattering domain (CSD)) size was evaluated from the width of X-ray diffraction peaks using the Scherrer formula:

$$d = \frac{k\lambda}{(B - b)\cos\theta}, \quad (4)$$

where  $k = 0.89$  is the Scherrer constant,  $\lambda = 1.5406 \text{ \AA}$  is the X-ray wavelength used,  $B$  is the full width ( $2\theta$ ) at half maximum of the diffraction peak,  $b$  is instrumental broadening ( $2\theta$ ), and  $\theta$  is the Bragg angle.

MSR was conducted at atmospheric pressure in a conventional tubular reactor (tube length, 21.5 cm; inner diameter, 0.9 cm) in the temperature range 200–400°C. A sample of a catalyst (weighing 0.3 g) was mixed with granulated quartz (size fraction 1–3 mm) and placed in the central part of the reactor. The reactor was heated to the required temperature by an electric furnace, while the catalyst was exposed to flowing argon (20 mL/min). The temperature in the reactor was measured by a Chromel–Alumel thermocouple. Prior to each series of experiments, the catalyst was reduced with a  $H_2$  (5%) + Ar flow (20 mL/min) at a temperature of 350°C for 3 h. A liquid mixture of methanol with water (stoichiometric molar ratio of 1 : 1) was fed to an evaporator using an Instalar 1488 Dixon infusion pump. The unreacted water and alcohol were condensed in a glass receiver cooled to +1°C. The composition of the uncondensed reaction products was determined on an LKhM 8MD gas chromatograph using a thermal conductivity detector, helium carrier gas, and columns packed with a Porapak T stationary phase (for water, methanol, and other oxygenates) and activated carbon (for CO and  $CO_2$ ). The hydrogen and methane concentrations in the reaction products were determined on a Chrom-4 chromatograph equipped with a thermal conductivity detector and zeolite column (CaA Zeosorb phase, Ar carrier gas). Chromatograms were analyzed using Ecochrom software.

Methanol conversion  $X$  (mol %) and reforming selectivity ( $S$ , %) were assessed from the analytical data using the following equations:

$$X_{CH_3OH} = \frac{n_{CH_3OH,in} - n_{CH_3OH,out}}{n_{CH_3OH,in}} \times 100\%, \quad (5)$$

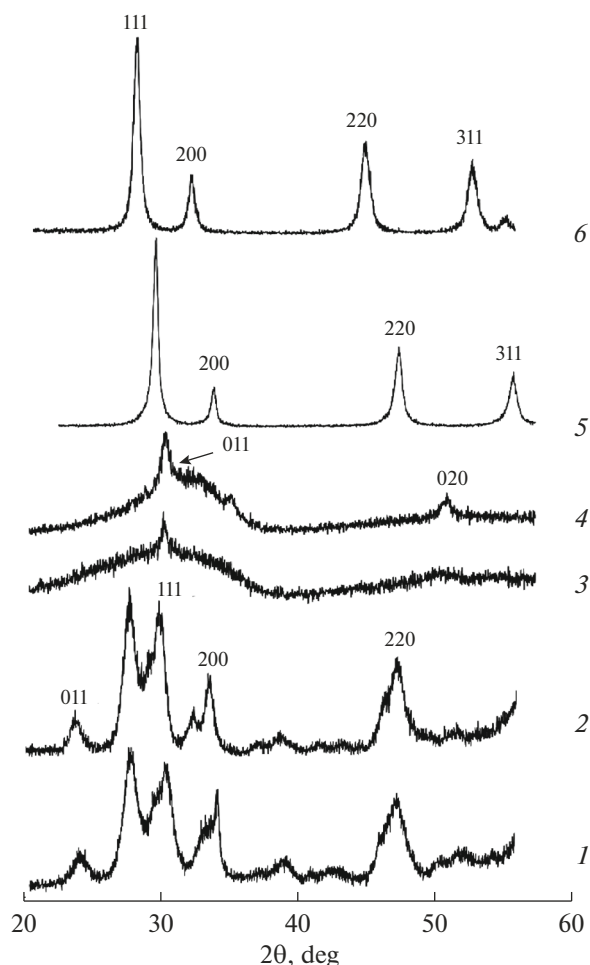


**Fig. 1.** Partial X-ray diffraction patterns of the materials annealed at 400°C: (1) ZrO<sub>2</sub>, (2) ZrO<sub>2</sub>-SnO<sub>2</sub>, (3) ZrO<sub>2</sub>-Nb<sub>2</sub>O<sub>5</sub>, (4) ZrO<sub>2</sub>-ZnO, (5) ZrO<sub>2</sub>-Y<sub>2</sub>O<sub>3</sub>, (6) CeO<sub>2</sub>-SnO<sub>2</sub>.

$$S = \frac{n_{\text{CO}_2, \text{out}}}{n_{\text{CO}_2, \text{out}} + n_{\text{CO}, \text{out}}} \times 100\%, \quad (6)$$

where  $n_{\text{CH}_3\text{OH}, \text{in}}$  and  $n_{\text{CH}_3\text{OH}, \text{out}}$  are the amounts of delivered and unreacted methanol, respectively, and  $n_{\text{CO}_2, \text{out}}$  and  $n_{\text{CO}, \text{out}}$  are the amounts of carbon dioxide and carbon monoxide in the reaction products. Product yields were evaluated as the amount of the corresponding reaction product (in moles) formed per gram of the metals present in the catalyst per hour. The gas hourly space velocity (GHSV), calculated as the ratio of the gas inflow rate (765 cm<sup>3</sup>/h) to the catalyst bed volume, was 172 h<sup>-1</sup>, and this parameter remained unchanged in all catalytic tests.

## RESULTS AND DISCUSSION

**Structural and morphological characteristics of the catalysts and support.** Figure 1 shows X-ray diffraction patterns of the samples after annealing at a tempera-

ture of 400°C. The observed reflections from the ZrO<sub>2</sub>-Y<sub>2</sub>O<sub>3</sub> and CeO<sub>2</sub>-SnO<sub>2</sub> samples can be indexed in cubic symmetry. Note that no lines attributable to tin oxide or yttria were detected, which suggested the formation of solid solutions (Fig. 1, scans 5, 6). It is worth noting that the lines of CeO<sub>2</sub> were slightly shifted to larger angles, due to the partial substitution of Sn<sup>4+</sup> cations, having a smaller ionic radius (0.69 Å), for Ce<sup>4+</sup> ions (0.97 Å) upon the formation of the solid solution. The cubic cell parameter of the CeO<sub>2</sub>-SnO<sub>2</sub> solid solution is 5.4018 ± 0.0009 Å, which is slightly smaller than the value characteristic of the cubic cell of undoped ceria (5.4111 Å). By contrast, doping with yttrium in the ZrO<sub>2</sub>-Y<sub>2</sub>O<sub>3</sub> system leads to an increase in the lattice parameter of ZrO<sub>2</sub> ( $a_{\text{ZrO}_2-\text{Y}_2\text{O}_3} = 5.1233$  Å) due to the substitution of Y<sup>3+</sup> cations, having a larger ionic radius (0.93 Å), for Zr<sup>4+</sup> (0.84 Å) and the formation of solid solutions.

In the case of tin doping of zirconia, the effect is much weaker. Like the undoped sample annealed at 400°C, this material crystallizes in monoclinic symmetry (Fig. 1, scans 1, 2). Note that its X-ray diffraction pattern shows reflections from both zirconia and tin oxide, pointing to lower tin solubility in the crystal lattice of zirconia.

After annealing at 400°C, the ZrO<sub>2</sub>-ZnO and ZrO<sub>2</sub>-Nb<sub>2</sub>O<sub>5</sub> samples had the form of poorly crystallized materials containing tetragonal zirconia nanoparticles and an X-ray amorphous phase, which was represented by a broad halo in the X-ray diffraction patterns of these samples (Fig. 1, scans 3, 4).

Raising the annealing temperature to 800°C led to the formation of monoclinic ZrO<sub>2</sub> in the zinc oxide-doped sample (Fig. 2, scan 1), but there was also a weak reflection corresponding to a tetragonal structure. In addition, zinc oxide was present as an individual phase, with well-defined reflections in the X-ray diffraction pattern of the sample.

In the niobium-doped system, after annealing at 800°C zirconia was present as a tetragonal phase (Fig. 2, scan 2). In addition, there were weak reflections from niobium oxide. Thus, in this case, niobium partially dissolved in zirconia to form an imperfect tetragonal structure.

Table 1 summarizes some characteristics of the synthesized supports (BET and X-ray diffraction results). There is a tendency for the specific surface area of the materials to decrease as a result of doping. At the same time, the crystallite size of the major oxide phase changes little. The particle size evaluated from BET data exceeds the crystallite size by one to two orders of magnitude, which is due to agglomeration of the nanoparticles. Raising the annealing temperature leads to the formation of a material with a smaller specific surface area and a considerably larger particle size (Table 1). In view of this, in preparing catalytic sys-

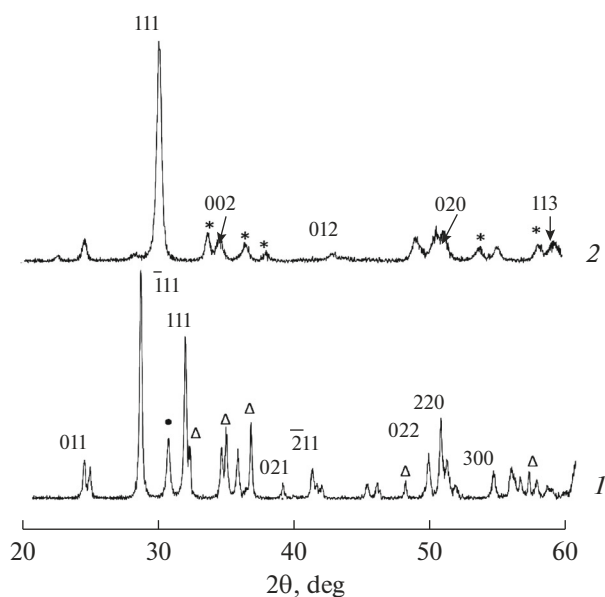


Fig. 2. Partial X-ray diffraction patterns of the samples annealed at 800°C: (1) ZrO<sub>2</sub>-ZnO, (2) ZrO<sub>2</sub>-Nb<sub>2</sub>O<sub>5</sub>.

tems we subsequently used supports annealed at 400°C.

The reflections in the X-ray diffraction pattern of Cu-Ni catalysts supported on oxide systems correspond to copper, which prevails in the composition of the catalysts (Fig. 3). At the same time, there is a well-defined shift of the reflections from copper, pointing to the formation of solid solutions. The cubic cell parameter of the Cu<sub>0.8</sub>-Ni<sub>0.2</sub> alloy obtained is  $3.6162 \pm 0.0007$  Å. It is also worth noting that the reflections from the metals are somewhat narrower than those from the oxide supports, suggesting that the particle size of the metals exceeds that of the supports. The crystallite size of the metals is about 20 nm, that is, about twice that of the supports.

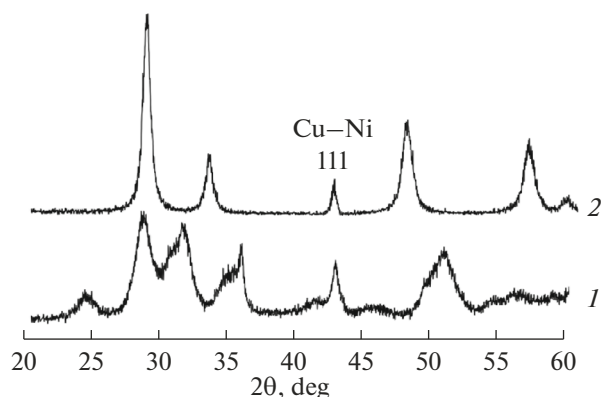


Fig. 3. X-ray diffraction patterns of the (1) Ni<sub>0.2</sub>-Cu<sub>0.8</sub>/ZrO<sub>2</sub> and (2) Ni<sub>0.2</sub>-Cu<sub>0.8</sub>/CeO<sub>2</sub>-SnO<sub>2</sub> catalysts.

#### Activity of the catalysts for the MSR process.

According to the present data, all of the materials studied have high selectivity in the intended reaction for hydrogen production: at least 99.5% for all of the catalysts even at high temperatures.

Figure 4 shows temperature dependences of the hydrogen yield and methanol conversion for the catalysts obtained in this study. The samples based on undoped zirconia and the Cu-Ni/CeO<sub>2</sub>-SnO<sub>2</sub> catalyst had the lowest catalytic activity. As shown earlier [31], the concentration of Ce<sup>4+</sup> and Ce<sup>3+</sup> cations on the surface of a catalyst determines in many respects the catalytic activity of composites. Note that a decrease in the amount of Ce<sup>3+</sup> cations relative to Ce<sup>4+</sup> led to a reduction in alcohol conversion and hydrogen yield. It seems likely that doping of ceria with tetravalent tin occurs to a significant degree on the particle surface and leads to a decrease in the surface concentration of trivalent cerium ions, which is responsible for the low catalytic activity of the resultant material. The Cu-Ni/ZrO<sub>2</sub>-SnO<sub>2</sub> sample also had relatively low activity, which can be interpreted as evidence that

Table 1. Specific surface area and characteristic particle sizes of the catalysts under study, evaluated from BET and X-ray diffraction results

Material	<i>S</i> , m <sup>2</sup> /g	Average particle size from BET data, nm	Crystallite size, nm	
			ZrO <sub>2</sub>	M <sub>x</sub> O <sub>y</sub>
ZrO <sub>2</sub>	155 ± 8	40	10 ± 1	—
CeO <sub>2</sub> -SnO <sub>2</sub> (10%)	75 ± 3	80	11 ± 1	—
ZrO <sub>2</sub> -Y <sub>2</sub> O <sub>3</sub> (10%)	52 ± 2	70	13 ± 1	—
ZrO <sub>2</sub> -SnO <sub>2</sub> (10%)	49 ± 2	120	8 ± 1	4 ± 2
ZrO <sub>2</sub> -ZnO (10%) (400°C)	59 ± 2	100	5 ± 2	—
ZrO <sub>2</sub> -ZnO (10%) (800°C)	14 ± 1	—	33 ± 1	24 ± 1
ZrO <sub>2</sub> -Nb <sub>2</sub> O <sub>5</sub> (10%) (400°C)	134 ± 4	45	8 ± 2	—
ZrO <sub>2</sub> -Nb <sub>2</sub> O <sub>5</sub> (10%) (800°C)	47 ± 2	—	12 ± 1	17 ± 1

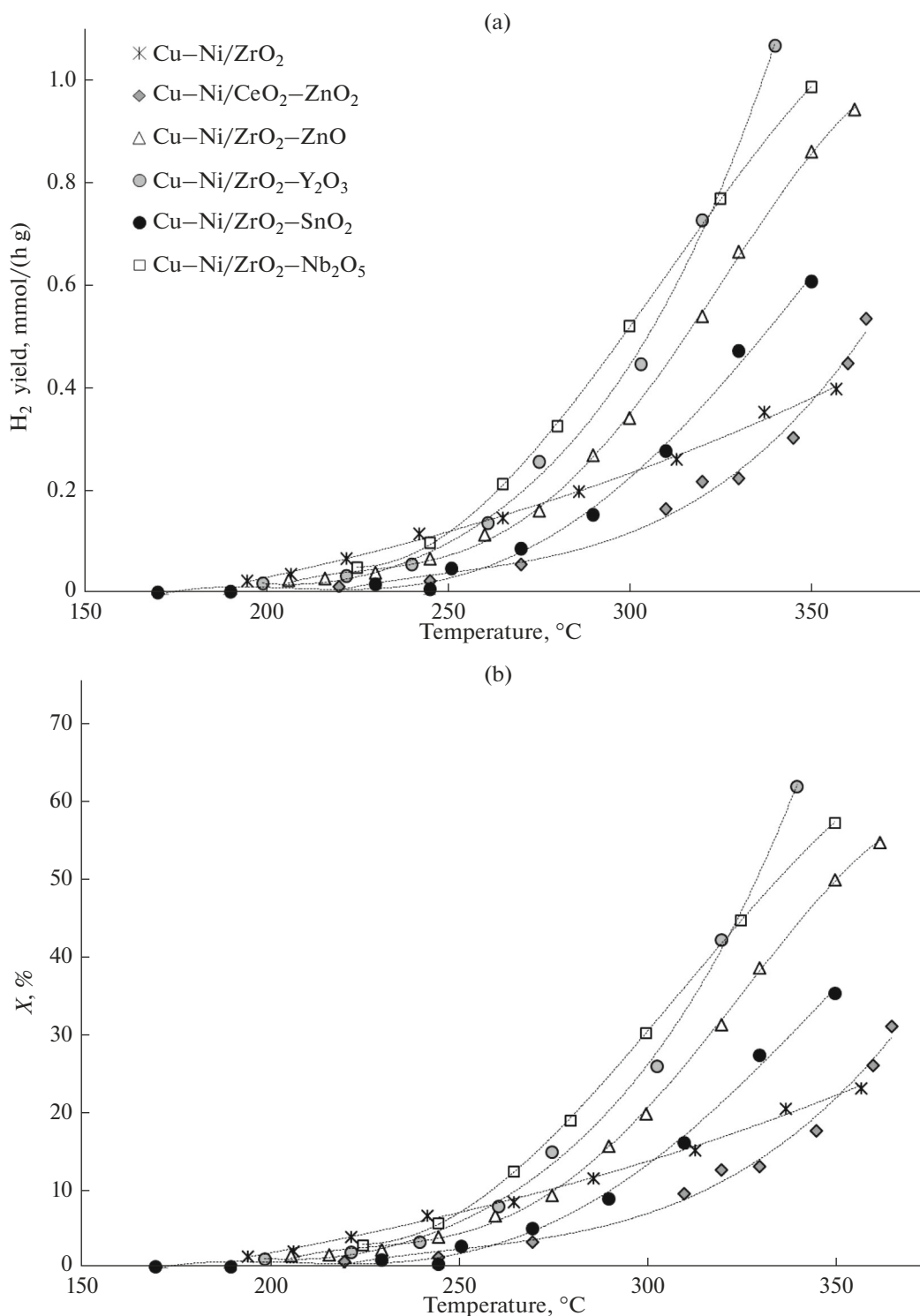


Fig. 4. Temperature dependences of the (a) H<sub>2</sub> yield and (b) methanol conversion for the catalysts obtained.

tin oxide has low water adsorption capacity. However, as was expected, no carbon dioxide was detected in reaction products to within the accuracy of chromatography even in high-temperature tests of the tin-doped samples.

The highest hydrogen yield was reached in the case of the samples doped with niobium and yttrium oxides. As shown above, the ZrO<sub>2</sub>-Y<sub>2</sub>O<sub>3</sub> and ZrO<sub>2</sub>-Nb<sub>2</sub>O<sub>5</sub> materials have a cubic and a tetragonal structure, respectively. This points to a higher activity of the

catalyst supported on the high-temperature  $\text{ZrO}_2$  polymorphs. The addition of trivalent or pentavalent metal ions leads to higher disorder and mobility in the oxygen sublattice of the oxide and increases the number of active centers, presumably due to structural defects, on the catalyst surface. Moreover, Table 1 demonstrates that the specific surface area of the niobium oxide-containing support is considerably larger, which can be interpreted as evidence for higher activity of the catalyst supported on the finer oxide particles.

## CONCLUSIONS

The present results lead us to conclude that changes in the composition and structure of an oxide support can influence the activity of sorption centers, the tendency of the support toward oxygen and/or proton transport processes, and its ability to participate in redox processes. In all cases, the addition of heterovalent ions improved the catalytic activity of the samples in comparison with undoped zirconia, probably because of the higher disorder and mobility in the oxygen sublattice of the oxide, and increased the number of active centers, presumably due to structural defects, on the catalyst surface.

A higher lattice symmetry of oxide supports allows a higher hydrogen yield to be reached in the MSR process catalyzed by Cu–Ni materials. Catalytic activity has been shown to increase in the sequence Cu–Ni/ $\text{ZrO}_2$  (monoclinic) < Cu–Ni/ $\text{ZrO}_2$ – $\text{SnO}_2$  (monoclinic) < Cu–Ni/ $\text{ZrO}_2$ – $\text{ZnO}$  (monoclinic) < Cu–Ni/ $\text{ZrO}_2$ – $\text{Nb}_2\text{O}_5$  (tetragonal)  $\approx$  Cu–Ni/ $\text{ZrO}_2$ – $\text{Y}_2\text{O}_3$  (cubic).

## FUNDING

This work was supported by the Russian Federation Ministry of Science and Higher Education (agreement no. RFMEFI58617X0053) and CNRS, France (project no. 38200SF).

## REFERENCES

1. Yaroslavtsev, A.B., Stenina, I.A., Kulova, T.L., Skundin, A.M., and Desyatov, A.V., *Nanomaterials for electrical energy storage*, *Comprehensive Nanoscience and Nanotechnology*, Andrews, D.L. et al., Eds., Amsterdam: Academic, 2019, 2nd ed., pp. 165–206.
2. Shafiei, E., Davidsdottir, B., Leaver, J., Stefansson, H., and Asgeirsson, E.I., Energy, economic, and mitigation cost implications of transition toward a carbon-neutral transport sector: a simulation-based comparison between hydrogen and electricity, *J. Clean Prod.*, 2017, vol. 141, pp. 237–247.
3. Moliner, R., Lazaro, M.J., and Suelves, I., Analysis of the strategies for bridging the gap towards the hydrogen economy, *Int. J. Hydrogen Energy*, 2016, vol. 41, pp. 19 500–19 508.
4. Abe, J.O., Popoola, A.P.I., Ajenifuja, E., and Popoola, O.M., Hydrogen energy, economy and storage: review and recommendation, *Int. J. Hydrogen Energy*, 2019, vol. 44, pp. 15 072–15 086.
5. Naruki, E., Shimoda, E., Goshome, K., Yamane, T., Nozu, T., and Maeda, T., Construction and operation of hydrogen energy utilization system for a zero emission building, *Int. J. Hydrogen Energy*, 2019, vol. 44, pp. 14 596–14 604.
6. Miranda, P.E., *Hydrogen energy, Sustainable and Perennial Science and Engineering of Hydrogen-Based Energy Technologies*, Miranda, P.E., Ed., Amsterdam: Academic, 2019, chapter 1, pp. 1–38.
7. Frusteri, F. and Bonura, G., *Hydrogen production by reforming of bio-alcohols*, *Compendium of Hydrogen Energy. Hydrogen Production and Purification*, Subramani, V. et al., Eds., Woodhead Publishing Series in Energy, 2015.
8. Ghasemzadeh, K., Jalilnejad, E., Mohamad, S., and Tilebon, S., *Hydrogen production technologies from ethanol*, *Ethanol*, Basile, A. et al., Eds., Amsterdam: Elsevier, 2019, chapter 12, pp. 307–340.
9. López-Tenllado, F.J., Hidalgo-Carrillo, J., Montes-Jiménez, V., Sánchez-López, E., Urbano, F.J., and Marinas, A., Photocatalytic production of hydrogen from binary mixtures of C-3 alcohols on Pt/ $\text{TiO}_2$ : influence of alcohol structure, *Catal. Today*, 2019, vol. 328, pp. 2–7.
10. Li, Sh., Zheng, H., Zheng, Y., Tian, J., Jing, T., Chang, Jo-Sh., and Ho, Sh.H., Recent advances in hydrogen production by thermo-catalytic conversion of biomass, *Int. J. Hydrogen Energy*, 2019, vol. 44, pp. 14266–14278.
11. Chiu, Y.J., Chiu, H.C., Hsieh, R.H., Jang, J.H., and Jiang, B.Y., Simulations of hydrogen production by methanol steam reforming, *Energy Proc.*, 2019, vol. 156, pp. 38–42.
12. Lytkina, A.A., Orekhova, N.V., and Yaroslavtsev, A.B., Catalysts for the steam reforming and electrochemical oxidation of methanol, *Inorg. Mater.*, 2018, vol. 54, no. 13, pp. 1315–1329.
13. Kim, D.H., Kim, J.H., Jang, Y.S., and Kim, J.C., Hydrogen production by oxidative steam reforming of methanol over anodic aluminum oxide-supported Cu–Zn catalyst, *Int. J. Hydrogen Energy*, 2019, vol. 44, pp. 9873–9882.
14. Tahay, P., Khani, Y., Jabari, M., Bahadoran, F., and Safari, N., Highly porous monolith/ $\text{TiO}_2$  supported Cu, Cu–Ni, Ru, and Pt catalysts in methanol steam reforming process for  $\text{H}_2$  generation, *Appl. Catal., A*, 2018, vol. 554, pp. 44–53.
15. Khzouz, M., Gkanas, E.I., Du, S., and Wood, J., Catalytic performance of Ni–Cu/ $\text{Al}_2\text{O}_3$  for effective syngas production by methanol steam reforming, *Fuel*, 2018, vol. 232, pp. 672–683.
16. Kuo, M.T., Chen, Y.Y., Hung, W.Y., Lin, S.F., Lin, H.P., Hsu, C.H., Shih, H.Y., Xie, W.A., and Li, S.N., Synthesis of mesoporous CuFe/silicates catalyst for methanol steam reforming, *Int. J. Hydrogen Energy*, 2019, vol. 44, pp. 14 416–14 423.
17. Sa, S., Silva, H., Brandao, L., Sousa, J.M., and Mendes, A., Catalysts for methanol steam reforming—a review, *Appl. Catal., B*, 2010, vol. 99, pp. 43–57.

18. Azenha, C.S.R., Mateos-Pedrero, C., Queirós, S., Concepción, P., and Mendes, A., Innovative ZrO<sub>2</sub>-supported CuPd catalysts for the selective production of hydrogen from methanol steam reforming, *Appl. Catal., B*, 2017, vol. 203, pp. 400–404.
19. Sarafráz, M.M., Safaei, M.R., Goodarzi, M., and Ajo-mandi, M., Reforming of methanol with steam in a micro-reactor with Cu–SiO<sub>2</sub> porous catalyst, *Int. J. Hydrogen Energy*, 2019 (in press). <https://doi.org/10.1016/j.ijhydene.2019.05.215>
20. Hwang, B.Y., Sakthinathan, S., and Chiu, T.W., Production of hydrogen from steam reforming of methanol carried out by self-combusted CuCr<sub>1-x</sub>Fe<sub>x</sub>O<sub>2</sub> ( $x = 0-1$ ) nanopowders catalyst, *Int. J. Hydrogen Energy*, 2019, vol. 44, pp. 2848–2856.
21. Thyssen, V.V., Sartore, D.M., and Assaf, E.M., Effect of preparation method on the performance of Ni/MgOSiO<sub>2</sub> catalysts for glycerol steam reforming, *J. Energy Inst.*, 2019, vol. 92, pp. 947–958.
22. Liu, X., Men, Y., Wang, J., He, R., and Wang, Y., Remarkable support effect on the reactivity of Pt/In<sub>2</sub>O<sub>3</sub>/MO<sub>x</sub> catalysts for methanol steam reforming, *J. Power Sources*, 2017, vol. 364, pp. 341–350.
23. Wang, S., Niu, H., Guo, M., Wang, J., Chen, T., and Wang, G., Effect of zirconia polymorph on the synthesis of diphenyl carbonate over supported lead catalysts, *Mol. Catal.*, 2019, vol. 468, pp. 117–124.
24. Lytkina, A.A., Zhilyaeva, N.A., Ermilova, M.M., Orekhova, N.V., and Yaroslavtsev, A.B., Influence of the support structure and composition of Ni–Cu-based catalysts on hydrogen production by methanol steam reforming, *Int. J. Hydrogen Energy*, 2015, vol. 40, pp. 9677–9684.
25. Liu, X., Toyir, J., Piscina, P.R., and Homs, N., Hydrogen production from methanol steam reforming over Al<sub>2</sub>O<sub>3</sub>- and ZrO<sub>2</sub>-modified CuZnOGa<sub>2</sub>O<sub>3</sub> catalysts, *Int. J. Hydrogen Energy*, 2017, vol. 42, pp. 13704–13711.
26. Guangwei, X., Laitao, L., Changquan, L., and Xiaomao, Y., Synthesis of mesoporous ZnO (m-ZnO) and catalytic performance of the Pd/m-ZnO catalyst for methanol steam reforming, *Energy Fuels*, 2009, vol. 23, pp. 1342–1346.
27. Sanches, S.G., Huertas Flores, J., and Pais da Silva, M.I., Cu/ZnO and Cu/ZnO/ZrO<sub>2</sub> catalysts used for methanol steam reforming, *Mol. Catal.*, 2018, vol. 454, pp. 55–62.
28. Stenina, I.A., Voropaeva, E.Yu., Brueva, T.R., Sinel'nikov, A.A., Drozdova, N.A., Ievlev, V.M., and Yaroslavtsev, A.B., Heat-treatment induced evolution of the morphology and microstructure of zirconia prepared from chloride solutions during, *Russ. J. Inorg. Chem.*, 2008, vol. 53, no. 6, pp. 842–848.
29. Borik, M.A., Volkova, T.V., Kuritsyna, I.E., Lomonova, E.E., Myzina, V.A., Ryabochkina, P.A., and Tabachkova, N.Yu., Features of the local structure and transport properties of ZrO<sub>2</sub>–Y<sub>2</sub>O<sub>3</sub>–Eu<sub>2</sub>O<sub>3</sub> solid solutions, *J. Alloys Compd.*, 2019, vol. 770, pp. 320–326.
30. Shukla, V., Balani, K., Subramaniam, A., and Omar, S., Phase stability and conductivity in the pseudo ternary system of xYb<sub>2</sub>O<sub>3</sub>–(12 – x)Sc<sub>2</sub>O<sub>3</sub>–88ZrO<sub>2</sub> ( $0 \leq x \leq 5$ ), *Solid State Ionics*, 2019, vol. 332, pp. 93–101.
31. Lytkina, A.A., Orekhova, N.V., Ermilova, M.M., and Yaroslavtsev, A.B., The influence of the support composition and structure (M<sub>x</sub>Zr<sub>1-x</sub>O<sub>2-d</sub>) of bimetallic catalysts on the activity in methanol steam reforming, *Int. J. Hydrogen Energy*, 2018, vol. 43, pp. 198–207.
32. Trovarelli, A., *Catalysis by Ceria and Related Materials*, London: Imperial College, 2002, p. 508.
33. Zhao, Q., Lorenz, H., Turner, S., Lebedev, O.I., Tendeloo, G.V., Rameshan, C., Klotzer, B., Konzett, J., and Penner, S., Catalytic characterization of pure SnO<sub>2</sub> and GeO<sub>2</sub> in methanol steam reforming, *Appl. Catal., A*, 2010, vol. 375, pp. 188–195.
34. Guarido, C.E.M., Cesar, D.V., Souza, M.M.V.M., and Schmal, M., Ethanol reforming and partial oxidation with Cu/Nb<sub>2</sub>O<sub>5</sub> catalyst, *Catal. Today*, 2009, vol. 142, pp. 252–257.
35. Dancini-Pontes, I., De Souza, M., Silva, F.A., Scaliant, M.H.N.O., Alonso, C.G., Bianchi, G.S., Neto, A.M., Pereira, G.M., and Fernandes-Machado, N.R.C., Influence of the CeO<sub>2</sub> and Nb<sub>2</sub>O<sub>5</sub> supports and the inert gas in ethanol steam reforming for H<sub>2</sub> production, *Chem. Eng. J.*, 2015, vol. 273, pp. 66–74.
36. Bejugama, S. and Pandey, A.K., Effect of Nb<sub>2</sub>O<sub>5</sub> on sintering and mechanical properties of ceria stabilized zirconia, *J. Alloys Compd.*, 2018, vol. 765, pp. 1049–1054.
37. Cai, F., Lu, P., Ibrahim, J.J., Fu, Y., Zhang, J., and Sun, Y., Investigation of the role of Nb on Pd–Zr–Zn catalyst in methanol steam reforming for hydrogen production, *Int. Hydrogen Energy*, 2019, vol. 44, pp. 11717–11733.
38. Stenina, I.A., Voropaeva, E.Yu., Veresov, A.G., Kapustin, G.I., and Yaroslavtsev, A.B., Effect of precipitation pH and heat treatment on the properties of hydrous zirconium dioxide, *Russ. J. Inorg. Chem.*, 2008, vol. 53, no. 3, pp. 350–356.

*Translated by O. Tsarev*